中国光学（中英文） Chinese Optics 核心期刊

基于表面等离子体共振的光子准晶体光纤甲烷氢气传感器

刘强 赵锦 孙宇丹 刘伟 王建鑫 刘超 吕靖薇 王诗淼 蒋宇 朱剑豪

A novel methane and hydrogen sensor with surface plasmon resonance-based photonic quasi-crystal fiber

LIU Qiang, ZHAO Jin, SUN Yu-dan, LIU Wei, WANG Jian-xin, LIU Chao, LV Jing-wei, WANG Shi-miao, JIANG Yu, PAUL K CHU

引用本文:
刘强, 赵锦, 孙宇丹, 刘伟, 王建鑫, 刘超, 吕靖薇, 王诗淼, 蒋宇, 朱剑豪. 基于表面等离子体共振的光子准晶体光纤甲烷氢气传感器[J]. 中国光学, 2023, 16(1): 174−183. doi: 10.37188/CO.EN.2022−0006
LIU Qiang, ZHAO Jin, SUN Yu-dan, LIU Wei, WANG Jian-xin, LIU Chao, LV Jing-wei, WANG Shi-miao, JIANG Yu, PAUL K CHU. A novel methane and hydrogen sensor with surface plasmon resonance-based photonic quasi-crystal fiber[J]. *Chinese Optics*, 2023, 16(1): 174-183. doi: 10.37188/CO.EN.2022-0006

在线阅读 View online: https://doi.org/10.37188/CO.EN.2022−0006

文章编号 2097-1842(2023)01-0174-10

A novel methane and hydrogen sensor with surface plasmon resonance-based photonic quasi-crystal fiber

LIU Qiang[1], ZHAO Jin[1], SUN Yu-dan[1,2], LIU Wei[1], WANG Jian-xin[1], LIU Chao[1*], LV Jing-wei[1], WANG Shi-miao[1], JIANG Yu[1], PAUL K CHU[3]

(1. *School of Physics and Electronics Engineering*, *Northeast Petroleum University*, *Daqing* 163318, *China*;
2. *College of Mechanical and Electrical Engineering*, *Daqing Normal University*, *Daqing* 163712, *China*;
3. *Department of Physics*, *City University of Hong Kong*, *Tat Chee Avenue*, *Hong Kong* 999077, *China*)

* *Corresponding author*, *E-mail*: *msm-liu@126.com*

Abstract: A novel Photonic Quasi-crystal Fiber (PQF) sensor based on Surface Plasmon Resonance (SPR) is designed for simultaneous detection of methane and hydrogen. In the sensor, Pd-WO_3 and cryptophane E doped polysiloxane films deposited on silver films are the hydrogen and methane sensing materials, respectively. The PQF-SPR sensor is analyzed numerically by the full-vector finite element method and excellent sensing performance is demonstrated. The maximum and average hydrogen sensitivities are 0.8 nm/% and 0.65 nm/% in the concentration range of 0% to 3.5% and the maximum and average methane sensitivities are 10 nm/% and 8.81 nm/% in the same concentration range. The sensor has the capability of detecting multiple gases and has large potential in device miniaturization and remote monitoring.

Key words: methane sensor; hydrogen sensor; surface plasmon resonance; photonic quasi-crystal fiber

收稿日期:2022-04-12; **修订日期**:2022-05-09

基金项目:海南省重点研发计划(No. ZDYF2022GXJS003); 东北石油大学青年科学基金(No. 2019QNL-17); 黑龙江省博士后科研发展基金(No. LBH-Q20081); 中央地方高校改革发展人才培养资助项目; 香港城市大学战略研究资助项目(SRG)(No. 7005505)

Supported by the Hainan Province Science and Technology Special Fund (No. ZDYF2022GXJS003); Youth Science Foundation of Northeast Petroleum University (No. 2019QNL-17); Postdoctoral Scientific Research Development Fund of Heilongjiang Province (No. LBH-Q20081);Local Universities Reformation and Development Personnel Training Supporting Project from Central Authorities, City University of Hong Kong Strategic Research Grant (SRG) (No. 7005505)

基于表面等离子体共振的光子准晶体光纤甲烷氢气传感器

刘　强[1], 赵　锦[1], 孙宇丹[1,2], 刘　伟[1], 王建鑫[1], 刘　超[1*],
吕靖薇[1], 王诗淼[1], 蒋　宇[1], 朱剑豪[3]
(1. 东北石油大学 物理与电子工程学院, 黑龙江 大庆 163318;
2. 大庆师范学院 机电工程学院, 黑龙江 大庆 163712;
3. 香港城市大学 物理系, 香港 999077)

摘要: 设计了一种用于同时检测甲烷和氢气的基于表面等离子体共振 (SPR) 的新型光子准晶体光纤 (PQF) 传感器。在该传感器中, 在银膜上分别沉积 Pd-WO_3 和掺杂聚硅氧烷的笼型分子 E 薄膜作为氢气和甲烷的敏感材料。采用全矢量有限元方法对 PQF-SPR 传感器进行数值分析, 结果证明该传感器具有良好的传感性能。在 0%~3.5% 的浓度范围内, 氢气的最大检测灵敏度和平均灵敏度分别为 0.8 nm/% 和 0.65 nm/%, 甲烷的最大灵敏度和平均灵敏度分别为 10 nm/% 和 8.81 nm/%。该传感器具有同时检测多种气体的能力, 在设备小型化和远程监测方面具有很大的潜力。

关　键　词: 甲烷传感器; 氢气传感器; 表面等离子体共振; 光子准晶体光纤
中图分类号: O433　　**文献标志码:** A　　**doi:** 10.37188/CO.EN.2022-0006

1　Introduction

Methane and hydrogen are flammable and potentially explosive gases and it is important to detect methane and hydrogen at the same time in industrial production and other applications. There are several types of electrical sensors to monitor hydrogen and methane but they are not suitable for the industrial environment due to the potential risks of sparks and explosion[1]. Optical fiber sensors can overcome the shortcomings as they have the advantages of small size, fast response, electrical insulation, corrosion resistance, and electromagnetic interference resistance. At present, several types of optical fiber sensors have been developed for gas sensing[2-4]. The Fiber Bragg Grating (FBG) sensor has the wavelength multiplexing capability but relatively lower sensitivity[5], whereas the interferometric optical fiber sensor has better sensitivity but poor stability[6]. Compared to these sensors, optical fiber sensors based on Surface Plasmon Resonance (SPR) have high sensitivity, low production cost, and remote on-line monitoring capability[7-10].

The SPR phenomenon which can be described in terms of collective oscillations of the free electron plasma at the interface between the metal and dielectric medium has been applied to refractive index sensing[11-14]. However the conventional prism-SPR sensor is too bulky. Aiming at the above problem, the miniature SPR sensors composed of optical fibers have been designed. For example, Wei *et al*.[15] have proposed a Long-Period Fiber Grating (LPFG) surface plasmon resonance sensor coated with a silver film and graphene monolayer for methane detection, the detection sensitivity is 0.344 nm/%. Liu *et al*.[16] have designed a Photonic Crystal Fiber (PCF) SPR sensor with a large side-hole structure. A gold film and Pd-WO_3 and Ultra-Violet Curable Fluoro-Siloxane (UVCFS) nano-films incorporated with cryptophane A are used to enhance the sensitivity of hydrogen and methane to achieve a sensitivity of 0.19 nm/% for hydrogen and 1.99 nm/% for methane. Liu *et al*.[17] have designed a methane sensor based on the long-period grating in photonic crystal fiber. By taking advantages of the LPFG and PCF-SPR, the methane sensitivity is 6.39 nm/%. However, the researches about SPR

sensors with the ability of simultaneous detection of methane and hydrogen are rarely reported.

In this work, a Photonic Quasi-crystal Fiber (PQF) based on SPR is designed to detect methane and hydrogen at the same time. PQF is a kind of microstructured optical fiber which are ordered but not periodic structures that lack translational symmetry but include rotational symmetry. Compared with PCF, the PQF exhibits similar properties such as endlessly single mode, flattened dispersion[18-19], high nonlinearity[20], large effective mode area[21] , high birefringence and so on. The structure includes two separate sensitive layers, and nano silver films are deposited on the D-shape surface and outside surface of the PQF. The methane and hydrogen sensitive films are coated on the silver films respectively to exploit the SPR effect. Our results show that the sensor has a high sensitivity of 10 nm/% for methane and 0.8 nm/% for hydrogen.

2 Modeling and analysis

The cross-section of the PQF-SPR sensor is shown in Fig. 1 (Color online). The basic structure is based on the simple six-fold quasi-crystal configuration with a lattice pitch Λ=2.5 μm and air hole diameter d=1.58 μm. To enhance the SPR effect, the three central air holes marked by the dotted line in Fig. 1 are removed to form a larger fiber core and two air holes are added to confine the core mode and reduce the transmission loss. The four top air holes are removed to form the D-shape region as the methane gas channel with a height of h_2=2.17 μm. The sensor can be fabricated by laser etching, 3D printing or pouring[22-23]. The silver film with a thickness of t_2 = 30 nm can be deposited on the flat surface by Chemical Vapor Deposition (CVD)[24] or magnetron sputtering[25]. The polysiloxane nanofilm with cryptophane E can be coated on Ag film as the methane sensitive materials by capillary impregnation coating[16] to avoid oxidation of silver. The thickness is t_CH_4=500 nm. In the same way, the Ag film and hydrogen sensitive film Pd-WO_3 are coated on the external surface of the PQF. The thicknesses are t_1=30 nm and t_H_2=250 nm. The outer layer is a perfectly matched layer and the background materials in the PQF are silica. The sensor is covered by a Perfectly Matched Layer (PML) with a diameter of 20 μm. As the concentration of hydrogen and methane increases, the refractive indexes of the hydrogen-sensitive film and methane-sensitive film decrease linearly in the range of 0%−3.5%. The functional relationships are described in equations (1) and (2)[16, 26], where C_H_2 and C_CH_4 represent the concentration of hydrogen and methane respectively.

$$n_1 = 1.995 - 0.000\,67\,C\_H_2 \quad , \qquad (1)$$

$$n_2 = 1.448 - 0.004\,6\,C\_CH_4 \quad . \qquad (2)$$

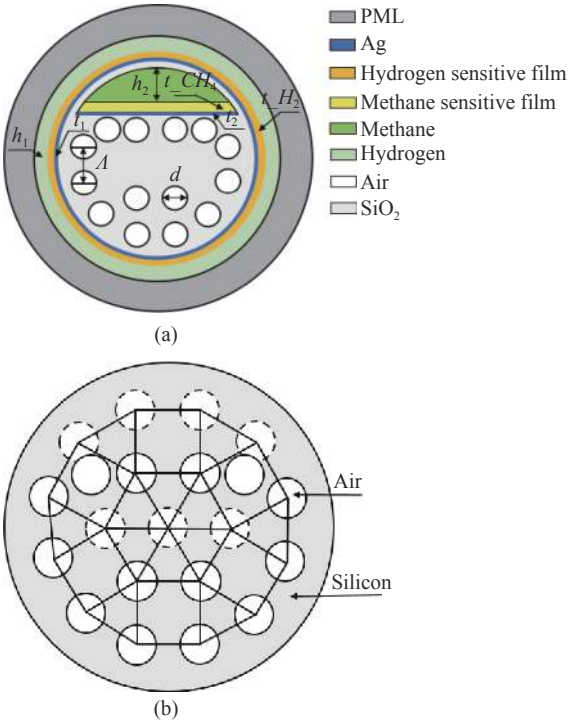

Fig. 1 Cross-section of the PQF-SPR sensor

The dispersion relationship of background material is determined by Eq. (3), where A_1= 0.696 166 300, A_2=0.407 942 600, A_3=0.897 479 400, B_1=0.068 404 3 μm², B_2=0.116 241 4 μm², B_3= 9.896 161 μm²[27]. In addition, the Drude-Lorentz model is used to describe the dielectric constant of sil-

ver and expressed in Eq. (4), where ε_∞=2.48 is the high frequency dielectric constant, ω_p=1.35×10^{16} (rad/s) is the plasma frequency, and ω_d=7.62×10^{13}(rad/s) is the damping frequency[28]:

$$n^2(\lambda) = 1 + \frac{A_1\lambda^2}{\lambda^2 - B_1^2} + \frac{A_2\lambda^2}{\lambda^2 - B_2^2} + \frac{A_3\lambda^2}{\lambda^2 - B_3^2} \quad , \quad (3)$$

$$\varepsilon(\omega) = \varepsilon_\infty - \frac{\omega_p^2}{\omega(\omega + i\omega_d)} \quad . \quad (4)$$

The calculation of confinement loss (CL) is shown in Eq. (5)[29]:

$$\alpha_{\text{loss}} = 8.686 \times \frac{2\pi}{\lambda} \text{Im}(n_{\text{eff}}) \times 10^4 \,(\text{dB/cm}) \quad , \quad (5)$$

where Im(n_{eff}) represents the imaginary part of the effective refractive index of the core mode.

3　Simulation and analysis

For a hydrogen concentration of 2.5%, the dispersion relationships of the X-polarized core mode and Surface Plasmon Polariton (SPP) mode are calculated and plotted in Fig. 2 (Color online) as red square dots and circular dots, respectively. It is evident that the phase matching condition of SPR is achieved at the cross point when resonance is the strongest. This is verified by the core mode and SPP mode field diagrams for X-polarization in Fig. 2(b). The power of the core mode is transferred to the SPP mode and therefore, the peak of the confinement loss spectra appears at the phase matching point as shown by the black curve in Fig. 2. The peak wavelength is 1 848.2 nm. Figs. 2(a) and 2(c) also show the electric field distributions of the X-polarized core mode and SPP mode at 1 875 nm. The resonance intensity is weakened as the wavelength is changed. The blue curve represents the confinement loss of Y-polarization. It is evident that the coupling intensity of X-polarization is much larger than that of Y-polarization due to the asymmetry of the structure. Therefore the confinement loss of X-polarization is chosen to analyze hydrogen sensing characteristics. Similarly, the SPR effect induced by the methane is shown in Fig. 3. The Y-polarized mode is adopted to calculate the confinement loss spectrum for methane since the methane-sensitive film is coated on the polished plane in the *Y* direction[30-31]. The peak wavelength of the confinement loss spectrum is 1 513 nm for a methane concentration of 2.5%. Fig. 3(b) shows the electric field distributions of the Y-polarized core mode and SPP mode at the phase matching point and Figs. 3(a) and 3(c) correspond to wavelength detuning of 1 570 nm. The confinement loss spectra of the PQF-SPR sensor exhibit two peaks at different wavelengths for hydrogen and methane and so simultaneous detection of methane and hydrogen can be accomplished.

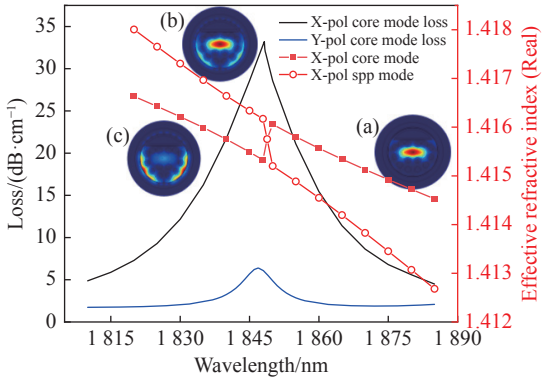

Fig. 2　Dispersion relationships of the X-polarized core mode and SPP mode, confinement loss spectra, and electric field distributions for *C_H*$_2$=2.5%: (a) X-polarized core mode at 1875 nm, (b) X-polarized core mode at the phase matching point, and (c) X-polarized SPP mode at 1875 nm.

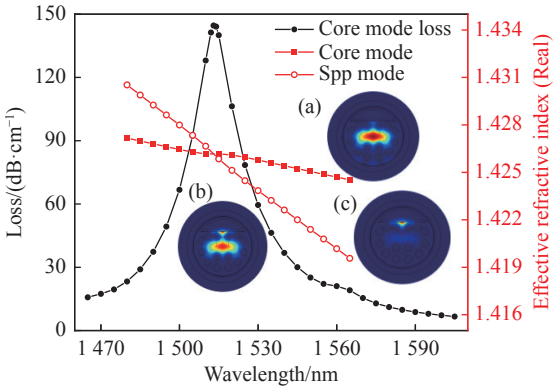

Fig. 3　Dispersion relationships of the Y-polarized core mode and SPP mode, confinement loss spectra, and electric field distributions for *C_CH*$_4$=2.5%: (a) Y-polarized core mode at 1 570 nm, (b) Y-polarized core mode at the phase matching point, and (c) Y-polarized SPP mode at 1570 nm.

The SPR sensor is very sensitive to the refractive index of the surrounding environment[32]. The refractive indexes of the hydrogen-sensitive film and methane-sensitive film change with hydrogen and methane concentrations, and therefore the position and peak intensity of SPR generated by coupling between the Ag film and core mode change accordingly. The sensitivity of the sensor can be determined by the wavelength interrogation method as shown in the following[33]:

$$S(\lambda)=\frac{\Delta\lambda_{\text{peak}}}{\Delta C_{\text{gas}}}(\text{nm}/\%) \quad , \qquad (6)$$

where $\Delta\lambda_{\text{peak}}$ represents the variation of the resonance wavelength with changing gas concentration and ΔC_{gas} represents the variation of gas concentration.

From the safety point of view, the performance of the sensor is studied in the concentration range of 0%−3.5% for hydrogen and methane. For d=1.58 μm, Λ=2.5 μm, t_1=30 nm, t_2=30 nm, h_1=1.5 μm, h_2=2.17 μm, t_H_2=250 nm, and t_CH_4=500 nm, the variations of the confinement loss spectra with hydrogen and methane concentration are shown in Fig. 4 (Color online). With increasing hydrogen concentration, the confinement loss spectra of the X-polarized core mode move slowly to the short wavelength direction as shown in Fig. 4(a). The relationship between the resonance wavelength and hydrogen concentration is displayed in Fig. 5 (Color online). The resonance wavelength decreases linearly in the range of 0%−3.5%. The sensor achieves the highest hydrogen sensitivity of 0.8 nm/% in the range of 0.5%−1% and 3%−3.5%. Meanwhile, the average sensitivity is 0.65 nm/% according to the linear fitting in Eq. (7). In the same way, the confinement loss spectra of different methane concentrations are shown in Fig. 4(b). The results show that the methane has higher loss peak, narrower linewidth, and greater wavelength shift than hydrogen. The maximum sensitivity is 10 nm/% for methane concentration ranges of 0%−1% and 2%−2.5% and the average sensitivity is 8.81 nm/% according to Eq. (8). The R-square values (R^2) of the linear fitting curves for hydrogen and methane are 0.998 and 0.999, respectively, indicating that the relationship between the refractive index and gas concentration can be fitted well.

$$y_1=-0.01-0.65x_1 \quad , \qquad (7)$$

$$y_2=-0.58-8.81x_2 \quad . \qquad (8)$$

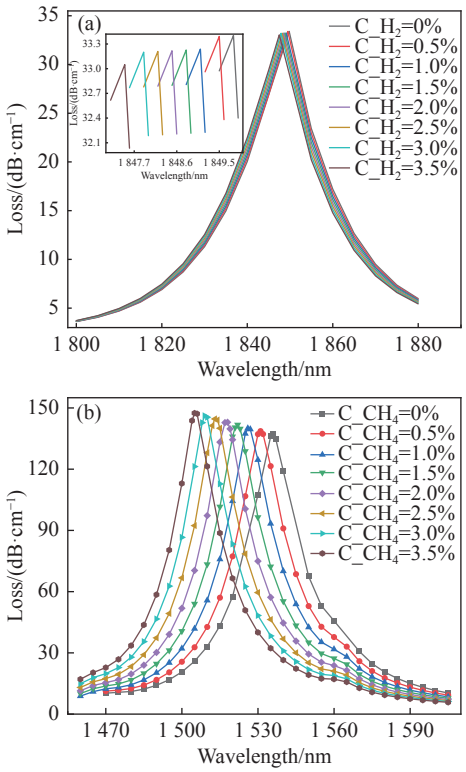

Fig. 4 CL spectra of the core mode for (a) hydrogen and (b) methane with different concentrations

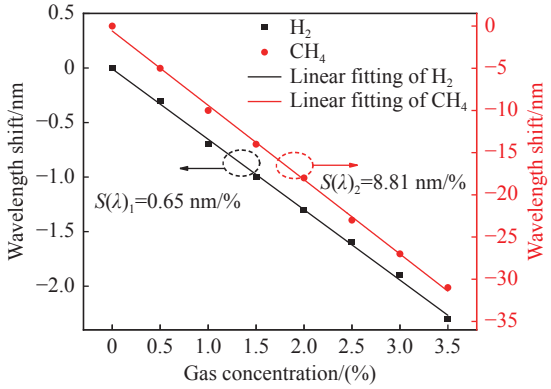

Fig. 5 Relationship between the gas concentration and wavelength shift for hydrogen and methane

The performance of the sensor can be optimized by changing the structural parameters. For a hy-

drogen concentration of 3%, the CL spectra for different air hole diameters d are shown in Fig. 6(a) (Color online). The resonance peak blue-shifts with increasing of air hole diameters. A larger d changes the effective refractive index of the core mode and shifts the phase matching point[34]. In order to optimize d, Fig. 6(b) (Color online) shows the relationship between the resonance wavelength and hydrogen concentration for different air hole diameters d, and the results exhibit a similar monotonic trend. The average sensitivity of the sensor is calculated by linear fitting and d=1.58 μm is the optimal air hole diameter to attain the maximum average hydrogen sensitivity.

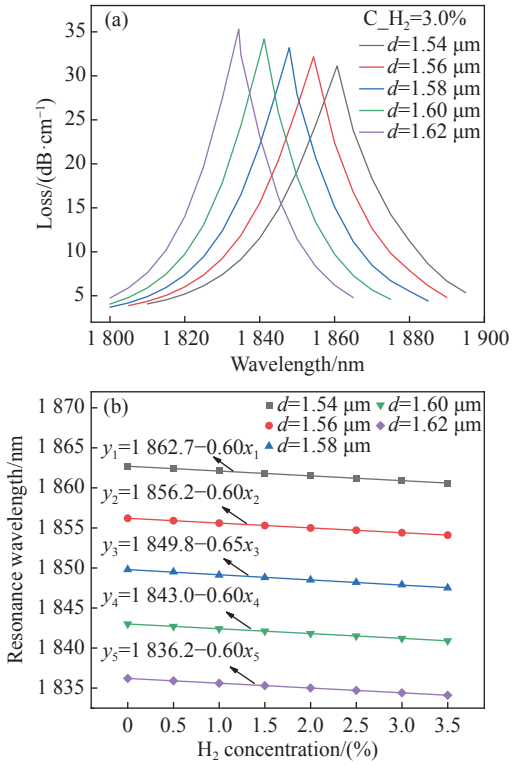

Fig. 6　(a) CL spectra of the core mode for different air hole diameters d when the hydrogen concentration is 3.0%. (b) Resonance wavelength versus hydrogen concentration (t_1=t_2=30 nm, h_1=1.5 μm, h_2=2.17 μm, and C_H_2=3%)

By using the same structural parameters, the sensitivity of the sensor for methane is analyzed as shown in Fig. 7(a) (Color online). The loss spectra blue-shifts and the resonance peaks decrease greatly with increasing air hole diameter d for methane concentrations of 2% and 2.5% because the Y-polarized core mode is better confined by a bigger air hole and energy leakage is less[34-35]. Fig. 7(b) shows the variation trend of the sensor with different air hole diameters as the methane concentration is changed from 0% to 3.5%. The slope of the linear fitting represents the average sensitivity of the sensor. It can be seen that the maximum sensitivity is obtained at d=1.58 μm and therefore d=1.58 μm is selected as the optimal air hole diameter.

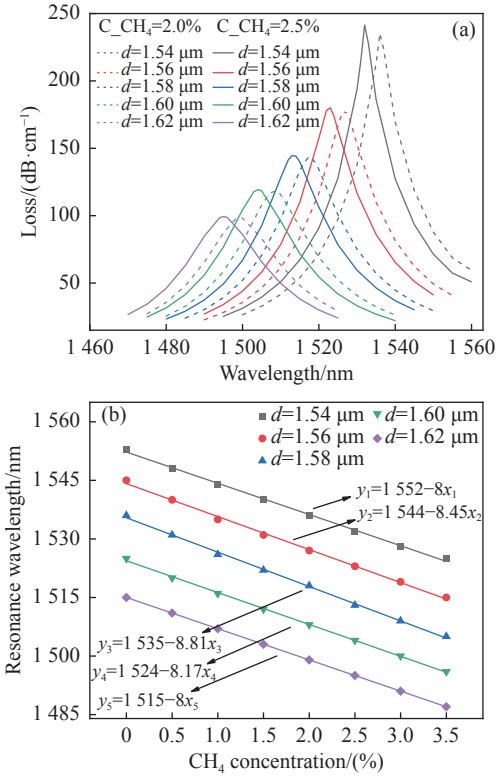

Fig. 7　(a) CL spectra of the core mode for different air hole diameters d when the methane concentrations are 2.0% and 2.5%. (b) Resonance wavelength versus methane concentration and average sensitivity (t_1=t_2=30 nm, h_1=1.5 μm, and h_2=2.17 μm).

The thickness of the metal film is optimized. When the silver film thickness is changed from 28 nm to 32 nm, the confinement loss spectra for C_H_2=3% is shown in Fig. 8(a) (Color online). The confinement loss spectra move to a longer wavelength with increasing Ag film thickness because a thicker silver film requires a longer wavelength to excite surface plasmon resonance[36]. At the same time, increasing the thickness of the silver film enhances the resonance between the core mode and

SPP mode and subsequently the resonance peak. Fig. 8(b) (Color online) shows the relationship between the resonance wavelength and hydrogen concentration for different silver film thicknesses. The slope of the curve indicates the average sensitivity which is calculated by linear fitting. The maximum average sensitivity is obtained when t_1= 30 nm. The impact of the silver film thickness on the methane confinement loss spectra is analyzed and shown in Fig. 9(a) (Color online). For methane concentrations of 2% and 2.5%, the spectra exhibit a significant blue-shift with increasing silver film thickness t_2. As the thickness is increased, the effective refractive index of the SPP mode decreases, but the effective refractive index of the core mode changes little, so that the phase matching point moves to a shorter wavelength[16]. At the same time, when the silver film thickness is large, the evanescent wave excited by evanescent field has more difficulty crossing the surface of the metal, resulting in the weakened SPR response[37]. Fig. 9(b) shows the average sensitivity of the sensor for different silver film thicknesses when the methane concentration is changed from 0% to 3.5%. The maximum sensitivity is observed for t_2=30 nm and hence, t_2=30 nm is the optimal parameter.

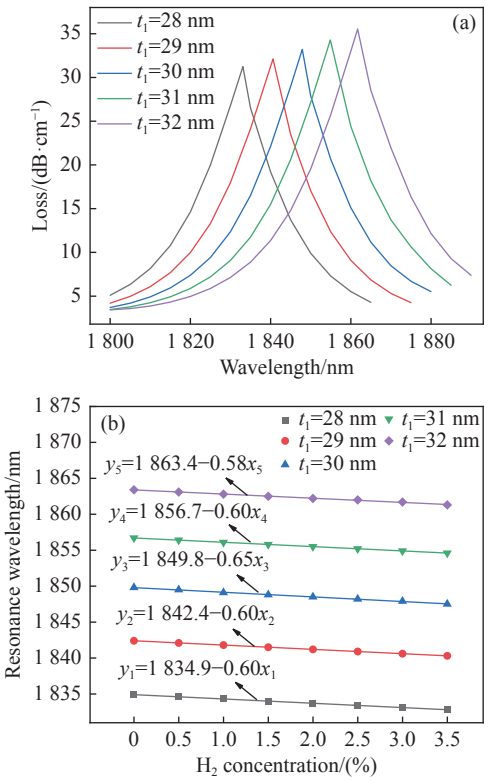

Fig. 8 (a) CL spectra of the core mode for different metal film thicknesses t_1 at a hydrogen concentration of 3.0%. (b) Resonance wavelength versus hydrogen concentration and average sensitivity (d=1.58 μm, t_2=30 nm, h_1=1.5 μm, and h_2=2.17 μm).

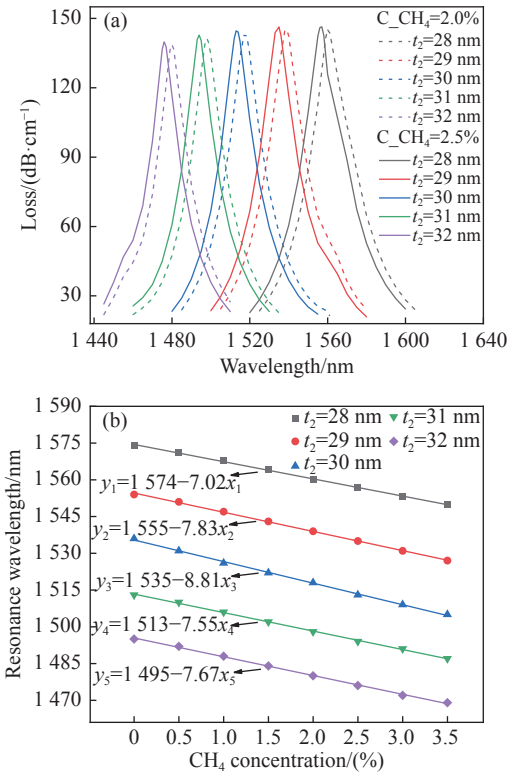

Fig. 9 (a) CL spectra of the core mode for different metal film thicknesses t_2 when the methane concentrations are 2.0% and 2.5%. (b) Resonance wavelength versus methane concentration and average sensitivity (d=1.58 μm, t_1=30 nm, h_1=1.5 μm, and h_2= 2.17 μm).

Finally the influence of the methane channel size on the sensor performance is analyzed and shown in Fig. 10 (Color online). When the height h_2 is increased from 1.97 μm to 2.37 μm, the confinement loss spectra move to a longer wavelength and the loss peak increases, because the height h_2 which determines the distance between the core and plasmonic materials influences the coupling efficiency of the core mode and SPP mode[34]. When the h_2 is increased, the distance between the silver film and fiber core is shorter so the resonance is stronger and loss peak is larger. Fig. 10 (b) shows the average sensitivity for different h_2 and the sensitivity reaches

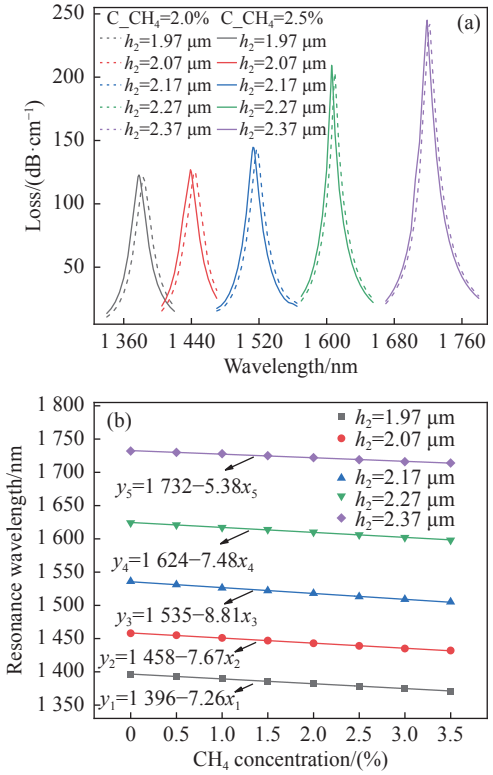

Fig. 10　(a) CL spectra of the core mode for the methane gas channel with different height h_2 when the methane concentrations are 2.0% and 2.5%. (b) Resonance wavelength versus methane concentration and average sensitivity (d=1.58 μm, t_1=t_2=30 nm, and h_1=1.5 μm).

the maximum for h_2=2.17 μm and therefore, h_2=2.17 μm is the optimal channel height.

4　Conclusion

A high-sensitivity methane and hydrogen sensor based on PQF-SPR is designed and analyzed. The two areas coated with Pd-WO_3 and cryptophane E doped polysiloxane are designed to detect hydrogen and methane, respectively. The sensor can be operated at different wavelengths to detect the two gases at the same time. The properties of the sensor is investigated by the finite element method and the numerical analysis result shows that the sensor has a maximum sensitivity of 0.8 nm/% and average sensitivity of 0.65 nm/% for hydrogen and maximum sensitivity of 10 nm/% and average sensitivity of 8.81 nm/% for methane. The sensor shows higher sensitivity in the gas concentration range between 0% and 3.5% and has great potential in gas detection. Moreover, the sensor structure and method can be further extended to detection of multiple gases and other fields.

References:

[1] HAO Q Q, LUO ZH M, WANG T, *et al*.. The flammability limits and explosion behaviours of hydrogen-enriched methane-air mixtures[J]. *Experimental Thermal and Fluid Science*, 2021, 126: 110395.

[2] SUMIDA S, OKAZAKI S, ASAKURA S, *et al*.. Distributed hydrogen determination with fiber-optic sensor[J]. *Sensors and Actuators B*:*Chemical*, 2005, 108(1-2): 508-514.

[3] YANG J CH, XU L J, CHEN W M. An optical fiber methane gas sensing film sensor based on core diameter mismatch[J]. *Chinese Optics Letters*, 2010, 8(5): 482-484.

[4] WANG Y, YANG M H, ZHANG G L, *et al*.. Fiber optic hydrogen sensor based on fabry-perot interferometer coated with sol-gel Pt/WO_3 coating[J]. *Journal of Lightwave Technology*, 2015, 33(12): 2530-2534.

[5] ZHOU B, CHEN ZH, ZHANG Y B, *et al*.. Active fiber gas sensor for methane detecting based on a laser heated fiber bragg grating[J]. *IEEE Photonics Technology Letters*, 2014, 26(11): 1069-1072.

[6] PUSTELNY T, MACIAK E, OPILSKI Z, *et al*.. Optical interferometric structures for application in gas sensors[J]. *Optica Applicata*, 2007, 37(1-2): 187-194.

[7] WANG X X, ZHU J K, XU Y Q, *et al*.. A novel plasmonic refractive index sensor based on gold/silicon complementary grating structure[J]. *Chinese Physics B*, 2021, 30(2): 024207.

[8] WANG X X, WU Y, WEN X L, *et al*.. Surface plasmons and SERS application of Au nanodisk array and Au thin film composite structure[J]. *Optical and Quantum Electronics*, 2020, 52(5): 238.

[9] LIU Q, JIANG Y, SUN Y D, *et al*.. Surface plasmon resonance sensor based on U-shaped photonic quasi-crystal fiber[J]. *Applied Optics*, 2021, 60(6): 1761-1766.

[10] LIU Q, SUN J D, SUN Y D, *et al*.. Surface plasmon resonance sensor based on photonic crystal fiber with indium tin

oxide film[J]. *Optical Materials*, 2020, 102: 109800.

[11] LI CH G, YAN B, LIU J J. Refractive index sensing characteristics in a D-shaped photonic quasi-crystal fiber sensor based on surface plasmon resonance[J]. *Journal of the Optical Society of America A*, 2019, 36(10): 1663-1668.

[12] YAN B, WANG A R, LIU E X, *et al*.. Polarization filtering in the visible wavelength range using surface plasmon resonance and a sunflower-type photonic quasi-crystal fiber[J]. *Journal of Physics D:Applied Physics*, 2018, 51(15): 155105.

[13] SIDDIK A B, HOSSAIN S, PAUL A K, *et al*.. High sensitivity property of dual-core photonic crystal fiber temperature sensor based on surface plasmon resonance[J]. *Sensing and Bio-Sensing Research*, 2020, 29: 100350.

[14] HOSSAIN B, ISLAM S M R, HOSSAIN K M T, *et al*.. High sensitivity hollow core circular shaped PCF surface plasmonic biosensor employing silver coat: a numerical design and analysis with external sensing approach[J]. *Results in Physics*, 2020, 16: 102909.

[15] WEI W, NONG J P, ZHANG G W, *et al*.. Graphene-based long-period fiber grating surface plasmon resonance sensor for high-sensitivity gas sensing[J]. *Sensors*, 2017, 17(1): 2.

[16] LIU H, WANG M, WANG Q, *et al*.. Simultaneous measurement of hydrogen and methane based on PCF-SPR structure with compound film-coated side-holes[J]. *Optical Fiber Technology*, 2018, 45: 1-7.

[17] LIU H, ZHANG Y Z, CHEN C, *et al*.. Transverse-stress compensated methane sensor based on long-period grating in photonic crystal fiber[J]. *IEEE Access*, 2019, 7: 175522-175530.

[18] LIU E X, LIANG SH W, LIU J J. Double-cladding structure dependence of guiding characteristics in six-fold symmetric photonic quasi-crystal fiber[J]. *Superlattices and Microstructures*, 2019, 130: 61-67.

[19] LIU E X, TAN W, YAN B, *et al*.. Robust transmission of orbital angular momentum mode based on a dual-cladding photonic quasi-crystal fiber[J]. *Journal of Physics D:Applied Physics*, 2019, 52(32): 325110.

[20] LEE Y S, LEE C G, KIM S. Annular core photonic quasi-crystal fiber with wideband nearly zero ultra-flat dispersion, low confinement loss and high nonlinearity[J]. *Optik*, 2018, 157: 141-147.

[21] SIVABALAN S, RAINA J P. High normal dispersion and large mode area photonic quasi-crystal fiber stretcher[J]. *IEEE Photonics Technology Letters*, 2011, 23(16): 1139-1141.

[22] LIU D M, LIU J CH, WANG H, *et al*.. Laser etching of groove structures with micro-optical fiber-enhanced irradiation[J]. *Nanoscale Research Letters*, 2012, 7(1): 318.

[23] ZHAO Q K, TIAN F J, YANG X H, *et al*.. Optical fibers with special shaped cores drawn from 3D printed preforms[J]. *Optik*, 2017, 133: 60-65.

[24] MARUYAMA T, FUKUI K. Indium-tin oxide thin films prepared by chemical vapor deposition[J]. *Journal of Applied Physics*, 1991, 70(7): 3848-3851.

[25] BING P B, SUI J L, WU G F, *et al*.. Analysis of dual-channel simultaneous detection of photonic crystal fiber sensors[J]. *Plasmonics*, 2020, 15(4): 1071-1076.

[26] ZHANG Y N, ZHAO Y, WANG Q. Measurement of methane concentration with cryptophane E infiltrated photonic crystal microcavity[J]. *Sensors and Actuators B:Chemical*, 2015, 209: 431-437.

[27] SHAKYA A K, SINGH S. Design of dual polarized tetra core PCF based plasmonic RI sensor for visible-IR spectrum[J]. *Optics Communications*, 2021, 478: 126372.

[28] YAN X, FU R, CHENG T L, *et al*.. A highly sensitive refractive index sensor based on a V-shaped photonic crystal fiber with a high refractive index range[J]. *Sensors*, 2021, 21(11): 3782.

[29] LIU Q, SUN J D, SUN Y D, *et al*.. High-sensitivity SPR sensor based on the eightfold eccentric core PQF with locally coated indium tin oxide[J]. *Applied Optics*, 2020, 59(22): 6484-6489.

[30] YANG ZH, XIA L, LI CH, *et al*.. A surface plasmon resonance sensor based on concave-shaped photonic crystal fiber for low refractive index detection[J]. *Optics Communications*, 2019, 430: 195-203.

[31] ZHAN Y S, LI Y L, WU ZH Q, *et al*.. Surface plasmon resonance-based microfiber sensor with enhanced sensitivity by gold nanowires[J]. *Optical Materials Express*, 2018, 8(12): 3927-3940.

[32] PAUL A K, HABIB S, HAI N H, *et al*.. An air-core photonic crystal fiber based plasmonic sensor for high refractive index sensing[J]. *Optics Communications*, 2020, 464: 125556.

[33] LIU Q, ZHAO J, SUN Y D, *et al*.. High-sensitivity methane sensor composed of photonic quasi-crystal fiber based on surface plasmon resonance[J]. *Journal of the Optical Society of America A*, 2021, 38(10): 1438-1442.

[34] GANGWAR R K, SINGH V K. Highly Sensitive surface plasmon resonance based D-shaped photonic crystal fiber refractive index sensor[J]. *Plasmonics*, 2017, 12(5): 1367-1372.

[35] HOSSAIN B, HOSSAIN S, ISLAM S M R, *et al*.. Numerical development of high performance quasi D-shape PCF-SPR biosensor: an external sensing approach employing gold[J]. *Results in Physics*, 2020, 18: 103281.

[36] HOSSAIN B, MAHENDIRAN T V, ABDULRAZAK L F, *et al*.. Numerical analysis of gold coating based quasi D-shape dual core PCF SPR sensor[J]. *Optical and Quantum Electronics*, 2020, 52(10): 446.

[37] LIANG H, SHEN T, FENG Y, *et al*.. A surface plasmon resonance temperature sensing unit based on a graphene oxide composite photonic crystal fiber[J]. *IEEE Photonics Journal*, 2020, 12(3): 7201811.

Author Biographics:

LIU Qiang (1980—), Male, born in Tailai, Heilongjiang, Ph.D, Professor, graduated from Harbin Engineering University in 2012, and is mainly engaged in optical fiber sensing technology. E-mail: nepulq @126.com

LIU Chao (1978 —), Male, born in Mulan, Heilongjiang, Ph.D, Professor, doctoral supervisor, graduated from Harbin Institute of Technology in 2008, and is mainly engaged in micro-structured optical devices. E-mail: msm-liu@126.com